Charge states of medium energy He ions scattered from rutile TiO_2(110) surfaces

K. Mitsuhara[1], T. Kano[2], Y. Yamamoto[1] and Y. Kido[2]

[1] The SR Center, Ritsumeikan University, Kusatsu, Shiga-ken 525-8577, Japan

[2] Department of Physics, Ritsumeikan University, Kusatsu, Shiga-ken 525-8577, Japan

Abstract

The charge state of medium energy He ions scattered from solid surfaces depends on emerging energy and angle as well as the surface materials. We measured He^+ fractions for 54 – 140 keV He^+ ions incident on rutile TiO_2(110) and scattered from the top-layer Ti atoms at the $[1\bar{1}0]$- and [001]-azimuth. The He^+ fractions measured at both azimuths were decreased with increasing emerging angle (scaled from surface normal) and saturated at ~75 and ~85° at the [001]- and $[1\bar{1}0]$-azimuth, respectively. The He^+ fractions for the $[1\bar{1}0]$-azimuth denoted by η^+_{110} were considerably larger by 10 - 20 % than those for the [001]-azimuth (η^+_{001}) at emerging angles below ~75° (non-equilibrated). The equilibrium He^+ fraction is close to the semi-empirical data given by Marion-Young. It was also found that the η^+_{110} values measured at emerging angle of ~80° were larger more than 20 % compared with the η^+_{001} values in the emerging energy range from 50 to 130 keV. Such a strong dependence on crystallographic orientation of scattering plane is simply explained by the atomic arrangements at the crystalline azimuths.

I. INTRODUCTION

Medium energy ion scattering spectrometry (MEIS) is a powerful tool for determining elemental depth profiles and atomic structures near surface regions[1-6]. For precise spectrum analysis, it is essential to have reliable data of energy loss (stopping power), energy straggling, line-shape and H^+ or He^+ fractions. Ziegler et al.[7] provided semi-empirical formulas for the energy loss of H and He ions in a wide energy range and in a matter of all elements, which have been widely used. However, the Ziegler's stopping power values sometimes deviate significantly from experimental values. Therefore, it is recommended to measure stopping power values employing a standard sample covered with a thin layer of interest, whose thickness was determined in advance by Rutherford backscattering using MeV He^+ ions[8]. Concerning the energy straggling, the Lindhard-Scharff formula[9] reproduces well MEIS spectra[10,11]. If one employs a spectrometer with an excellent energy resolution, the energy spectrum measured for He ions scattered from near surface atoms take an asymmetric profile with a lower energy tail because of excitations of electrons in the intermediate and outer shells during a large angle collision. This asymmetric line shape is well approximated by an exponentially modified Gaussian (EMG) distribution function[12,13]. In MEIS analysis, magnetic or electrostatic energy analyzers are employed and thus accurate values of H^+ and He^+ fractions are indispensable. They are dependent on emerging energy, emerging angle and surface material[14-17].

In this study, we have measured the He^+ fractions for 45 – 140 keV He^+ ions incident on rutile TiO_2(110) surface and scattered from the top-layer Ti atoms at the $[1\bar{1}0]$- and [001]-azimuth. Note that the atomic structure of the TiO_2(110) surface is well known. The He^+ fractions determined here are dependent on emerging angle and emerging energy at both scattering planes. It is also found that the He^+ fractions observed are clearly dependent on crystallographic orientation of scattering plane. The results obtained are simply explained by the atomic arrangement at the crystalline azimuths.

II. EXPERIMENTS AND SPECTRUM ANALYSIS

MEIS measurements were performed at the beamline 8 named SORIS working at Ritsumeikan SR Center[18]. A duoplasma ion source provided intense 5- 200 keV He^+ ion beams with a good emittance. The accelerated He^+ beams were well collimated to 0.18 mm in horizontal and 2.0 mm in vertical plane and then incident on a target sample which was mounted on a 6-axis goniometer. The sample was positively biased at +90 V to suppress secondary electron emission and the ion-irradiated area was shifted slightly to

avoid radiation damage after an integrated beam current of 1 μC. Scattered He^+ ions were energy-analyzed by deflection in a toroidal electrostatic field. The exact energy was measured with a position sensitive detector combined with a three-stage micro-channel plate. The detection efficiency ε and energy resolution $\Delta E/E$ (FWHM) of the toroidal analyzer were 0.44±0.02 and $9\pm1\times10^{-4}$, respectively[19].

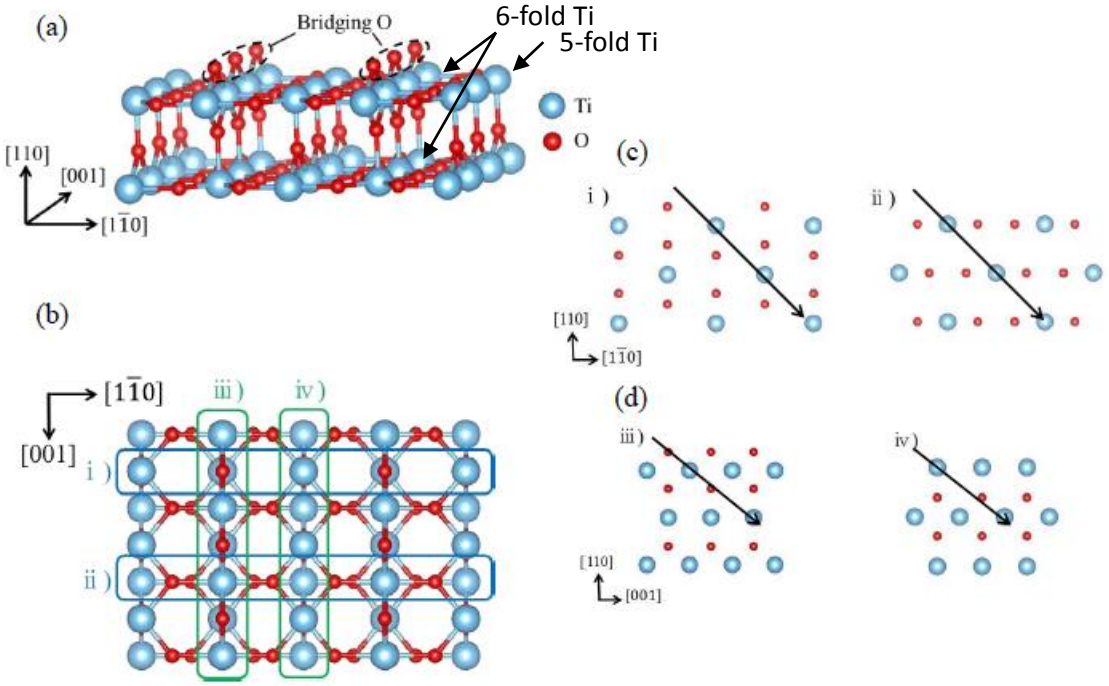

Fig. 1. (a) Ball and stick model for rutile TiO_2(110) surface. (b) Side view of TiO_2(110) surface. Frames (i) and (ii) correspond to two different Ti rows at $[1\bar{1}0]$-azimuth and (iii) and (iv) indicate two Ti rows at [001]-azimuth. (c) Side views for two scattering planes corresponding to (i) and (ii) at $[1\bar{1}0]$-azimuth. (d) Side views for two scattering planes corresponding to (iii) and (iv) at [001]-azimuth.

We purchased the TiO_2(110) substrates chemically etched and mirror-finished from Shinkosha corporation. Clean surfaces were obtained by annealing at 800°C for 30 min followed by repeating Ar^+-sputtering and annealing at 600°C in ultra-high vacuum (UHV). Such a treatment changed the color from transparency into dark-blue and led to conductivity due to increase in Ti interstitials acting as an electron donor. We confirmed a (1×1) ordered structure by reflective high energy electron diffraction. The surface consists of bridging O (O_{br}) rows and parallel aligned 5-fold Ti rows, which are illustrated schematically in Figs. 1(a)-(d)[20]. We measured energy spectra for He^+ ions incident along the $[0\bar{1}0]$-axis at the $[1\bar{1}0]$-azimuth and also along the $[1\bar{1}1]$-axis at the

[001]-azimuth. All the experiments were carried out *in situ* under UHV conditions ($\leq 2\times10^{-10}$ Torr).

The scattering yield from *n*-th layer atoms at an incident angle of θ_{in} is expressed by

$$Y_n = Q\ (d\sigma/d\Omega)\ n\Delta x\ \Delta\Omega\ \varepsilon\ \eta^+\ P_{CL}(n)/\cos\theta_{in}, \qquad (1)$$

where Q is number of He^+ incidence, $d\sigma/d\Omega$ scattering cross section, $n\Delta x$ number of target atoms (atoms/cm^2) and $\Delta\Omega$ solid angle subtended by the toroidal detector (7.64×10^{-5} str). The detection efficiency ε = 0.44 as mentioned before, η^+ is He^+ fraction of interest and $P_{CL}(n)$ is a close encounter probability normalized by the hitting probability for un-shadowed top layer atoms. We adopted the scattering cross sections given by Lee and Hart[21], which give good approximation for relatively large scattering angles. The close encounter probabilities were calculated by Monte Carlo (MC) simulations of ion trajectories assuming a structure model for the rutile TiO_2(110)[22]. We estimated the root mean square (rms) thermal vibration amplitudes for bulk O and Ti atoms $< u_b >$ based on the Debye model and assumed the enhanced vibration amplitude of $\sqrt{2} < u_b >$ for top layer atoms in the vertical direction. Here, the Debye temperature of 778 K for rutile was employed, which was determined by specific heat measurement[23].

As mentioned before, the energy spectrum for He ions scattered from near surface atoms is asymmetric due to excitations of outer and intermediate electrons. This leads to the spectrum with a tail on the lower energy side. The asymmetric line shape is well approximated by the EMG function[12,13] given by

$$f(E-E_{out}(n)) = \frac{1}{2\sigma_0}\exp[-\frac{1}{2\sigma_0}\{2(E-E_{out}(n))-\frac{\sigma_n^2}{\sigma_0}\}]\cdot\{1+erf(\frac{E-E_{out}(n)-\sigma_n^2/\sigma_0}{\sqrt{2}\sigma_n})\} \qquad (2)$$

where $E_{out}(n)$ is emerging energy calculated using stopping powers, σ_n is energy spread for the scattering component from *n*-th layer atoms and *erf* represents an error function. Asymmetric parameter σ_0 is given by CasP-version 5.0[24].

If the scattering cross sections, energy spread calculated from the Lindhard-Scharff formula, close encounter probabilities and line shapes are given, observed MEIS spectrum can be decomposed uniquely into scattering component from each atomic-layer. Best-fitting the simulated MEIS spectrum to the observed one determined the He^+ fraction for the scattering component from the top-layer Ti as well as stopping powers. Here, we assumed the Ziegler's stopping power multiplied by a constant which is a fitting parameter.

III. RESULTS AND DISCUSSION

Figures 2(a) and (b) show the MEIS spectra observed for He^+ ions incident along the $[0\bar{1}0]$-axis and scattered to 45° ([010]-axis) and 71.5° ([210]-axis), respectively. The observed MEIS spectra were best-fitted assuming the stopping power of $1.7 \cdot S_Z$ (S_Z: Ziegler's stopping power) and η^+ = 0.65 (45°) and 0.64 (71.5°) for the He ions scattered from the top-layer Ti atoms. Here, we used the asymmetric parameters σ_0 values of 117 and 123 eV, respectively for 122 and 131 keV He^+ impact on Ti given by CasP version 5.0[24].

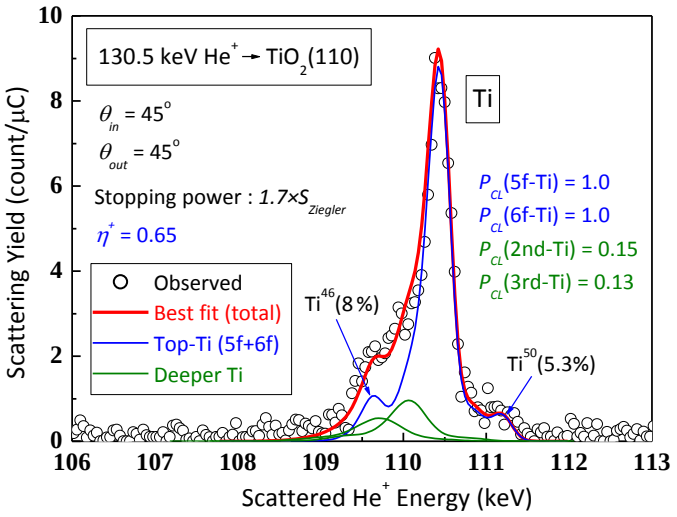

Fig. 2(a) MEIS spectrum observed for 131.3 keV He^+ ions incident along $[0\bar{1}0]$ -axis and scattered from Ti atoms to 45° ([010]-axis) with respect to surface normal. Red curve (thick) indicates best-fitted spectrum and blue and green curve (thin) denote scattering component from top-layer Ti and those from deeper layer Ti, respectively. (b) MEIS spectrum observed for 121.9 keV He^+ ions incident along $[0\bar{1}0]$ -axis and scattered to 71.5° ([210]-axis).

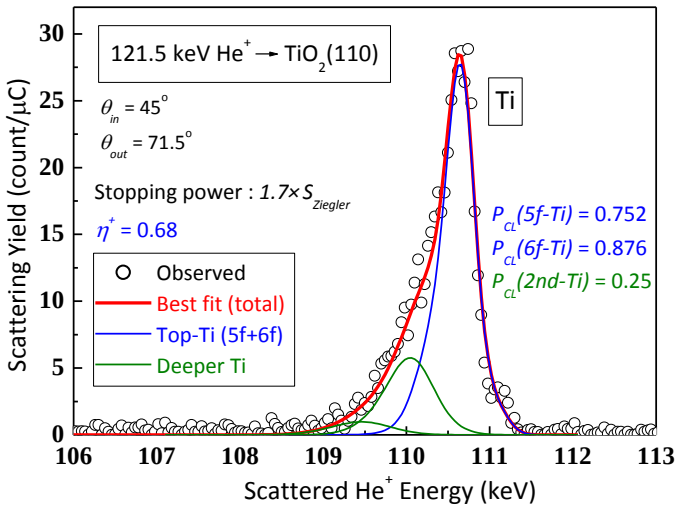

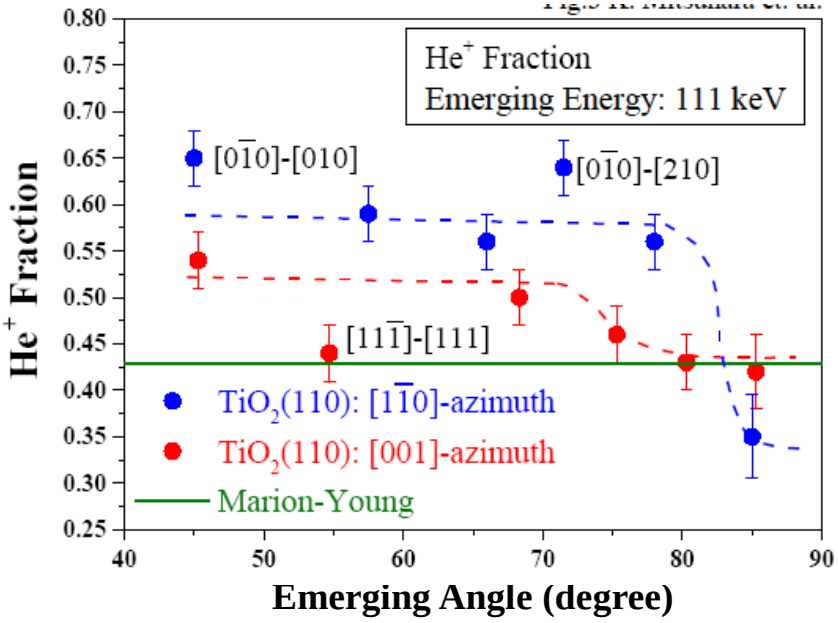

Fig. 3. He^+ fractions determined for $[1\bar{1}0]$ -azimuth (blue circles (open): η^+_{110}) and for [001]-azimuth (red circles (full): η^+_{001}) as a function of emerging angle. Emerging energy was fixed to 111 keV. Dashed curves were drawn to guide the eyes and straight line (green) denotes the equilibrium He^+ fraction given by Marion and Young[25].

Emerging angle dependence of He^+ fractions obtained for emerging energy fixed to 110 keV is shown in Fig. 3. The He^+ fractions determined for the $[1\bar{1}0]$- and [001]-azimuth, respectively are indicated by blue (open) and red (full) circles and denoted hereafter by η^+_{110} and η^+_{001}. Obviously, there is a trend that the η^+_{110} and η^+_{001} values decrease with increasing emerging angle (scaled from surface normal) and the latter reaches an equilibrium above 75º, which coincides with the equilibrated semi-empirical data given by Marion and Young (green straight line)[25]. In the case of the $[1\bar{1}0]$-azimuth, the η^+_{110} value seems to be equilibrated at an emerging angle around 85°. The non-equilibrated η^+_{110} values are larger by 10 - 20 % than the η^+_{001} values. Deviations of the η^+_{110} and η^+_{001} values from the smoothly fitted curves drawn to guide the eyes probably come from the assumed structure model[22] different significantly from a real structure. Indeed, the deviating three data were acquired under double alignment geometries, $[0\bar{1}0]$-incidence and [010]- and [210]-emergence and $[11\bar{1}]$ -incidence and [111]-emergence, which make the close encounter probabilities more sensitive to the surface structure than random emergence. Note that the rutile TiO_2(110)-1×1 surfaces prepared in the present experiment were reduced ones and may be slightly different from the stoichiometric surface. Another candidate for the deviations

is an ambiguity of energy loss, which depends on the positions of O atoms exposed to the vacuum and takes different values for He ions passing along the two types of atomic rows (see Fig. 1(b)). In fact, we estimated the energy loss values by MC simulations assuming the structure model reported by Parkinson et al.[22] and impact-parameter dependent stopping power given by CasP version 5.0[24]. This effect makes the spectrum shape from each atomic layer a little bit complicated and different from the EMG line shape. Therefore, it is inadequate to judge hastily the invalidity of the proposed structure model.

Emerging energy dependent He^+ fractions are indicated in Fig. 4, for both $[1\bar{1}0]$- and [001]-azimuth. The emerging angles for the $[1\bar{1}0]$- and [001]-azimuth were fixed to 78 and 80º, respectively. It is clear that the η^+_{110} values are considerably larger than the η^+_{001} values and the latter almost coincides with the data given by Marion-Young. Note that the η^+_{110} values are non-equilibrium ones, while the η^+_{001} values almost reach equilibrium. The difference between η^+_{110} and η^+_{001} becomes more pronounced with increasing emerging energy. Such a trend is also seen for smaller emerging angles (not shown here).

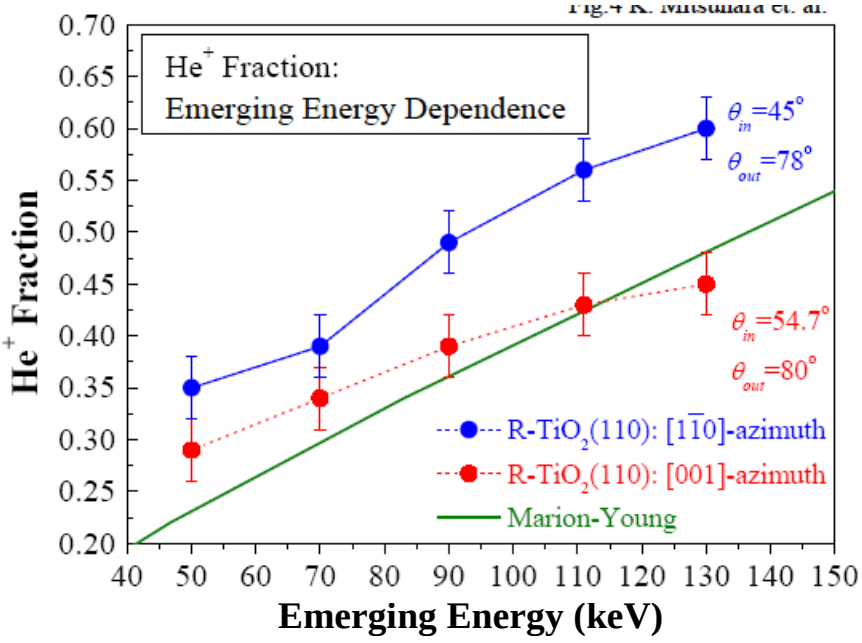

Fig. 4. He^+ fractions determined for $[1\bar{1}0]$-azimuth (blue circles (open): η^+_{110}) and for [001]-azimuth (red circles (full): η^+_{001}) as a function of emerging energy. He^+ ions were incident along $[0\bar{1}0]$-axis and scattered to 78° (random) at $[1\bar{1}0]$-azimuth and incident along $[11\bar{1}]$-axis and scattered to 80° at [001]-azimuth.

What leads to such a strong dependence on scattering (crystalline) plane ? As can be seen from the top view of the TiO_2(110) surface, the inter-atomic distance of Ti-Ti for the

$[1\bar{1}0]$-azimuth is more than twice that for the [001]-azimuth for both crystalline rows, in comparison between (i) and (iii) and between (ii) and (iv) (see Fig.1 (b)). For this reason, the He ions scattered from the top-layer Ti encounter more electrons in the intermediate and outer shells of Ti atoms in the rows ((iii) and (iv)) of the [001]-azimuth compared with the $[1\bar{1}0]$-azimuth. Also seen from Fig. 1(b), the inter-atomic distance between O_{br} atoms in the row of (i) is also more than twice that in the row of (iii). Note, here that a He ion immediately after a large angle collision has no bound electron because of the energy-time uncertainty. The collision time defined as the time lapse during a strong deflection of the trajectory in the large-angle collision is estimated roughly to be of the order of 10^{-17} sec, which results in an energy uncertainty of 100 – 200 eV exceeding the binding energy (54 eV) of the 1s electron of H^+ ion. The scattered He^{2+} ion experiences electron capture and loss processes, mainly capture processes before escaping from the surface[14,15]. Therefore, the He ions emerging at the $[1\bar{1}0]$-azimuth take a higher charge state than that for emergence at the [001]-azimuth. For large emerging angle, the charge state becomes equilibrium due to a long enough path length in the interacting region. According to the jellium model (homogeneous electron gas)[26], an electronic surface is expanded about a half monolayer from the top atomic plane toward the vacuum side. In the present energy region from 50 to 130 keV, primary charge states are He^0 (neutral) and He^+ and the fraction of He^{2+} is negligibly small less than 5 %[25]. The situation mentioned above explains clearly the reason why the η^+_{110} values are significantly larger than the corresponding η^+_{001} values. Of course, more quantitative discussion should be made based on quantum mechanical treatment despite its complexity. Recently, some efforts were reported for the charge exchange of low energy He ions at Cu(100) and Cu(110) surfaces based on the linear combination of atomic orbitals (LCAO) approach[27,28]. It is hopeful that such a quantum mechanical treatment is successfully extended to medium energy regime in the future.

IV. CONCLUSION

We determined the He^+ fractions (η^+) for He ions scattered from the top layer Ti of rutile TiO_2(110) surfaces at the $[1\bar{1}0]$- and [001]-azimuth. It was found that the η^+_{110} and η^+_{001} values decrease with increasing emerging angle and the latter reaches an equilibrium above ~75º, which coincides with the equilibrated semi-empirical data given by Marion and Young. In the case of the $[1\bar{1}0]$-azimuth, the η^+_{110} value seems to be equilibrated at emerging angle above ~85°. The non-equilibrated η^+_{110} values are larger 10 - 20 % than the η^+_{001} values. Concerning emerging energy dependence, the

non-equilibrated η^{+}_{110} values are considerably larger more than 20 % compared with the η^{+}_{001} values. The equilibrated η^{+}_{110} and η^{+}_{001} values coincide with the semi-empirical data given by Marion-Young within experimental uncertainties.

The reason why the non-equilibrated η^{+}_{110} values are significantly larger than the η^{+}_{001} values is attributed to the fact that the inter-atomic distances between Ti-Ti and O_{br}-O_{br} for the $[1\bar{1}0]$-azimuth are more than twice those for the [001]-azimuth. Therefore, the He ions scattered from top-layer Ti atoms at the [001]-azimuth encounter more electrons in the intermediate and outer shells of Ti and O_{br} atoms. A He ion immediately after a large angle collision has no bound electron because of the energy-time uncertainty. The scattered He^{2+} ion then undergoes electron capture and loss processes, mainly capture processes before escaping from the surface. For this reason, the He ions emerging at the $[1\bar{1}0]$-azimuth take a higher charge state than emergence at the [001]-azimuth.

ACKNOWLEDGEMENTS

The authors would like to thank their colleagues, T. Matsuda, M. Tagami and Y. Yoshida for their experimental support. This work was partly supported by the Ministry of Education, Japan, 'Academic Frontier Project'.

References

[1] J.F. van der Veen, Surf. Sci. Rep. **5** (1985) 199.

[2] J. Vrijmoeth, P.M. Zagwijn, J.W.M. Frenken, J.F. van der Veen, Phys. Rev. Lett. **67** (1991) 1134.

[3] K. Kimura, K. Nakajima, Y. Fujii, M. Mannami, Surf. Sci. **318** (1994) 363.

[4] P. Statiris, H.C. Lu, T. Gustafsson, Phys. Rev. Lett. **72** (1994) 3574.

[5] T. Nishimura, A. Ikeda, H. Namba and Y. Kido, Surf. Sci. **411** (1998) L834.

[6] P. Bailey, T.C.Q. Noakes, D.P. Woodruff, Surf. Sci. **426** (1999) 358.

[7] J.F. Ziegler, J.P. Biersack and U.L. Littmark, *The Stopping and Range of Ions in Solids*, (Pergamon Press, New York, 1985).

[8] T. Nishimura, K. Mitsuhara, A. Visikovskiy and Yoshiaki Kido, Nucl. Instrum. Methods **B 280** (2012) 5.

[9] J. Lindhard and M. Scharff, K. Dan. Vidensk. Selsk. Mat. Fys. Medd. **27** (1953) 1.

[10] Y. Kido and T. Koshikawa, Phys. Rev. **A 44** (1991) 1759.

[11] K. Mitsuhara, T. Matsuda, K. Tominaga, P.L. Grande, G. Schiwietz and Y. Kido, Phys. Rev. **A 87** (2013) 042901.

[12] P. L. Grande, A. Hentz, R. P. Pezzi, I. J. R. Baumvol and G. Schiwietz, Nucl. Instrum. and Method **B 256** (2007) 92.

[13] M. Hazama, Y. kitsudo, T. Nishimura, Y. Hoshino, P. L. Grande, G. Schiwietz and Y. Kido, Phys. Rev. B **78**(2008) 193402.

[14] Y. Kido, T. Nishimura and F. Fukumura, Phys. Rev. Lett. **82** (1999) 3352.

[15] T. Okazawa, K. Shibuya, T. Nishimura and Y. Kido, Nucl. Instrum. Methods **B 256** (2007) 1.

[16] Y. Kitsudo, K. Shibuya, T. Nishimura, Y. Hoshino, I. Vickridge and Y. Kido, Nucl. Instrum. Methods **B 267** (2009) 566.

[17] K. Mitsuhara, T. Kushida, H. Okumura, H. Matsumoto, A. Visikovskiy, Y. Kido, Surf. Sci. **604** (2010) L48.

[18] Y. Kido, H. Namba, T. Nishimura, A. Ikeda, Y. Yan and A. Yagishita, Nucl. Instrum. Methods **B 136-138** (1998) 798.

[19] Y. Kido, T. Nishimura, Y. Hoshino and H. Namba, Nucl. Instr. and Meth. **B 161–163** (2000) 371.

[20] U. Diebold, Surf. Sci. Rep. **48** (2003) 53.

[21] S.R. Lee and R.R. Hart, Nucl. Instrum. Methods **B 79** (1993) 463.

[22] G. S. Parkinson, M. A. Muňoz-M*á*rquez, P. D. Quinn, M. J. Gladys, R. E. Tanner, D. P. Woodruff, P. Bailey and T. C. Q. Noakes, Phys. Rev. **B 73** (2006) 245409.

[23] C.J. Howard, T.M. Sabine and F. Dickson, Acta. Cryst. **B 47** (1991) 462.

[24] http://www.helmholtz-berlin.de/people/gregor-schiwietz/casp_en.html.

[25] J.B. Marion and F. C. Young, *Nuclear Reaction Analysis - Graphs and Tables* (North-Holland, Amsterdam, 1968).

[26] N.D. Lang and W. Kohn, Phys. Rev. **B 3** (1970) 1215.

[27] Diego Valdés, J.M. Blanco, V.A. Esaulov and R.C. Monreal, Phys. Rev. Lett. **97** (2006) 047601.

[28] D. Goebl, D. Primetzhofer, E. Abad, R.C. Monreal and P. Bauer, Nucl. Instrum. Methods **B 317** (2013) 23.